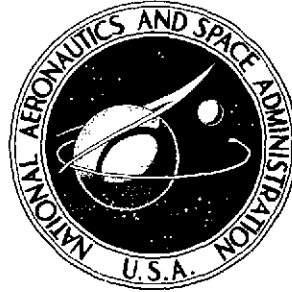


NASA TECHNICAL NOTE



NASA TN D-790

NASA TN D-7903

(NASA-TN-D-7903) - A PHOTOMETRIC FUNCTION FOR
DIFFUSE REFLECTION BY PARTICULATE MATERIALS
(NASA) 39 p HC \$3.75 CSSL 03B

N75-2223

Unclass
H1/91 19537

A PHOTOMETRIC FUNCTION FOR DIFFUSE REFLECTION BY PARTICULATE MATERIALS



Willard E. Meador and Willard R. Weaver

Langley Research Center

Hampton, Va. 23665



NATIONAL AERONAUTICS AND SPACE ADMINISTRATION • WASHINGTON, D. C. • APRIL 1975

1. Report No. NASA TN D-7903		2. Government Accession No.		3. Recipient's Catalog No.	
4. Title and Subtitle A PHOTOMETRIC FUNCTION FOR DIFFUSE REFLECTION BY PARTICULATE MATERIALS				5. Report Date April 1975	
				6. Performing Organization Code	
7. Author(s) Willard E. Meador and Willard R. Weaver				8. Performing Organization Report No. L-10021	
9. Performing Organization Name and Address NASA Langley Research Center Hampton, Va. 23665				10. Work Unit No. 185-50-51-01	
				11. Contract or Grant No.	
12. Sponsoring Agency Name and Address National Aeronautics and Space Administration Washington, D.C. 20546				13. Type of Report and Period Covered Technical Note	
				14. Sponsoring Agency Code	
15. Supplementary Notes					
16. Abstract A photometric function is proposed to describe the diffuse reflection of radiation by particulate materials. Both multiple scattering and the dominant effects of particle shadowing are included and the function is verified by comparisons with the photometries of laboratory surfaces. The function is a major improvement over the frequently used, strictly empirical, and much simpler Minnaert function in that brightness measurements of planetary and other diffusely scattering surfaces can be used to calculate the brightness for geometries other than those used in the measurements and for which the Minnaert function does not apply; the measurements also can be directly related to such surface characteristics as particle size, single-particle albedo, and compactness.					
17. Key Words (Suggested by Author(s)) Photometry for planetary surfaces Planetary surface properties Remote sensing			18. Distribution Statement Unclassified - Unlimited New Subject Category 91		
19. Security Classif. (of this report) Unclassified		20. Security Classif. (of this page) Unclassified		21. No. of Pages 37	22. Price* \$3.75

A PHOTOMETRIC FUNCTION FOR DIFFUSE REFLECTION

BY PARTICULATE MATERIALS

By Willard E. Meador and Willard R. Weaver
Langley Research Center

SUMMARY

A photometric function is proposed to describe the diffuse reflection of radiation by particulate materials. Both multiple scattering and the dominant effects of particle shadowing are included and the function is verified by comparisons with the photometries of laboratory surfaces. The function is a major improvement over the frequently used, strictly empirical, and much simpler Minnaert function in that brightness measurements of planetary and other diffusely scattering surfaces can be used to calculate the brightness for geometries other than those used in the measurements and for which the Minnaert function does not apply; the measurements also can be directly related to such surface characteristics as particle size, single-particle albedo, and compactness.

INTRODUCTION

The difficulty in obtaining in situ information about a planet makes it desirable to have a photometric function for planetary surfaces that describes the surface brightness as a function not only of the angles of incidence, emission, and phase, but also the physical properties of the material that forms the surface. The most commonly used photometric function for correlating and analyzing data on planetary surfaces and for describing the reflection from (or brightness of) planetary surfaces is the well-known Minnaert function. (See ref. 1.) The Minnaert function, however, has very insufficient basis in theory, is not derived from first principles, is restricted in validity to certain classes of scattering geometries, and, of considerable importance, cannot be used to interpret photometric behavior in terms of the physical properties of the reflecting surface.

In principle at least, photometric functions can be found from solutions to radiative transfer equations governing the passage of radiation between and through the particles comprising a particulate surface. Current transfer equations are restricted by the classical, and often inappropriate, simplifying assumption of sufficiently large interparticle separations for each particle to be in the far field for scattering by every other particle. (See ref. 2.) These equations, therefore, neglect the frequently important phenomenon of

mutual shadowing of the particles. Perhaps the best method to date for including mutual particle shadowing in radiative transfer theory is that of Irvine (ref. 3), who corrected the single-scattering term in a Neumann series solution in powers of the single-particle albedo. In such an approach the original transfer equation is not corrected. Since the transfer equations describing successive orders of scattering are closely coupled in the Neumann scheme, the use of a corrected first-order solution in the source function of the uncorrected second-order equation may yield important inconsistencies. As will be shown, an additional difficulty is present because the results of reference 3 do not approach the proper limit when applied to geometries involving grazing incidence or emission.

The purpose of the present paper is to propose and test a photometric function for diffuse reflection that allows direct determination of surface characteristics from measured brightness data. The function is a linear combination of a modification to Irvine's shadow-corrected, but otherwise exact, solution of the classical first-order transfer equation in the limit of very low albedo and Lambert's scattering law in the opposite limit of very high levels of multiple scattering. This approach has been proposed elsewhere (ref. 4) but without experimental verification and with earlier and less acceptable theories for the contribution of single scattering. The present research is the first to provide verification of this approach by comparisons with the experimental brightness of several laboratory surfaces.

Appearing in the equation for normalized brightness are three empirical parameters that are related to particle size, single-particle albedo, and compactness. These material properties are thus potentially determinable from comparisons of the function with photometric measurements. Laboratory measurements have shown that variations of these empirical parameters with changes in the properties of the surfaces are in good qualitative agreement with the theoretical interpretations.

SYMBOLS

A'	overlap area common to the cylinders of incidence and emission
A''	specific area (see eq. (A9))
a_0	photometric parameter in phase function
a_1	photometric parameter, C_2/C_1
a_2	packing factor, $n\rho^3$

B	parameter in equation (17)
C	proportionality factor, $I/\cos i$
C_1	parameter proportional to weight factor for single scattering
C_2	parameter proportional to weight factor for multiple scattering
F	net flux of impinging collimated radiation perpendicular to beam
f	shadowing-correction factor
G	function defined by equation (B10)
g	function defined by equation (A11)
H	function defined by equation (B9)
h	depth within scattering material
I	intensity of radiation perpendicular to beam reflected from a semi-infinite material
I_1	first-order radiation intensity
i	incident angle with respect to surface normal of impinging collimated radiation
J_1	function defined by equation (B11)
J_2	function defined by equation (B12)
K	volume absorption coefficient
k	Minnaert exponent
N	number of particles contained in volume V of particulate material
n	particle number density

P	probability that no particle center lies within volume v
p	phase function
S	volume scattering coefficient
V	total volume of particulate material
V'	total overlap volume of cylinders of incidence and emission
v	sum of volumes of two cylinders of cross-sectional area $\pi\rho^2$ that extend from a scattering particle at depth h within the material to the surface in the directions of incidence and emission
v'	overlap volume of two cylinders of cross-sectional area $\pi\rho^2$
v''	function defined by equation (A14)
x	integration variable (see eq. (A10))
α	phase angle between directions of incidence and emission
β	single particle albedo
γ	angle between η -axis and projection of h onto ηz -plane
δ	angular deviation from mirror-point geometry
ϵ	emission angle with respect to surface normal of observed scattered radiation
μ	function defined by equation (7)
ν	function defined by equation (8)
ξ, η, z	rectangular Cartesian coordinates (see fig. 8)
ρ	effective particle radius

- τ optical depth, $n\pi\rho^2h$
- Φ surface brightness (with shadowing) normalized to unity at $i = \epsilon = 0$
- Φ' surface brightness (without shadowing) normalized to unity at $i = \epsilon = 0$

Subscripts:

- 1 lower limit of integration
- 2 upper limit of integration

THEORETICAL DEVELOPMENT

Low-Albedo Limit

In the limit of very low albedo, the photometric function employed in this research will be required to approach (apart from shadowing corrections to be introduced subsequently) the exact solution of the following radiative transfer equation (ref. 3) for first-order (that is, single) scattering:

$$\cos \epsilon \frac{dI_1(\tau, i, \epsilon, \alpha)}{d\tau} = I_1(\tau, i, \epsilon, \alpha) - \frac{\beta F p(\alpha)}{4\pi} \exp\left(-\frac{\tau}{\cos i}\right) \quad (1)$$

where I_1 is the first-order radiation intensity at depth h within the material, i is the incident angle of the impinging collimated beam of net flux F , ϵ is the emission angle of the observed scattered radiation, α is the phase angle between the emission and incidence directions, τ is the optical depth $(K + S)h$, and K and S are the absorption and scattering coefficients, respectively. The phase function $p(\alpha)$ is defined so that $\beta p(\alpha)/4\pi$, where $\beta = S/(K + S)$ is the single-particle albedo, represents the fraction of the light incident on a particle that is scattered into a unit solid angle about a vector inclined at $\pi - \alpha$ radians from the incident direction. Hence, $p(\alpha)$ must satisfy the normalization condition

$$\int_0^\pi p(\alpha) \sin \alpha \, d\alpha = 2 \quad (2)$$

The solution of equation (1) for the intensity reflected from a semi-infinite, single-scattering material is

$$I_1(0, i, \epsilon, \alpha) = \frac{\beta F(K+S)p(\alpha)}{4\pi \cos \epsilon} \int_0^\infty \exp(-nv) dh = \frac{\beta Fp(\alpha) \cos i}{4\pi(\cos i + \cos \epsilon)} \quad (3)$$

where n is the particle number density and $v = (K+S) \left[(1/\cos i) + (1/\cos \epsilon) \right] h/n$. If the coefficient $K+S$ is equated to n times the cross-sectional area $\pi\rho^2$ corresponding to the effective particle radius ρ , then v becomes the sum of the volumes of two cylinders with cross-sectional areas $\pi\rho^2$ and with lengths equal to the distances between a scattering particle and the surface of the material, as measured along the directions of incidence and emission, respectively.

Equations (1) and (3) involve the implicit assumption that the particles comprising the scattering material are sufficiently far apart that each particle is in the far field for scattering by every other particle. Hence, the phenomenon of interparticle shadowing, which is important for most planetary surfaces, is not included. As shown in appendix A, Irvine (ref. 3) attempted to correct this deficiency by applying the principles of geometrical optics. Those results can be written in the following form for general scattering geometries:

$$I_1(0, i, \epsilon, \alpha) = \frac{\beta Fp(\alpha) \cos i}{4\pi(\cos i + \cos \epsilon)} f(i, \epsilon, \alpha, a_2) \quad (4)$$

where

$$f(i, \epsilon, \alpha, a_2) = e^{\mu-\nu} + \nu \int_0^1 \exp \left\{ \mu - \frac{\nu}{6\pi} \left[3\pi x + 2(2+x^2)(1-x^2)^{1/2} + 6x \sin^{-1} x \right] \right\} dx \quad (5)$$

$$a_2 = n\rho^3 \quad (6)$$

$$\mu = \frac{4a_2(1 + \cos \alpha)}{3 \sin \alpha} \quad (7)$$

and

$$\nu = \frac{\pi a_2 (\cos i + \cos \epsilon)}{\sin \alpha \cos i \cos \epsilon} \left[\sin^2 \alpha + 2(1 + \cos \alpha) \cos i \cos \epsilon \right]^{1/2} \quad (8)$$

The parameter a_2 is the packing factor of the material and $f(i, \epsilon, \alpha, a_2)$ is the shadowing-correction factor.

The model of reference 3 for single scattering is used in the present paper with two reservations. First, the radii of the incident and emission cylinders may be somewhat larger than the mean particle radius because of diffraction effects. The incident radiation aimed at a differential surface element of a given target particle will suffer losses by three mechanisms operating along its path starting at the surface of the material: absorption by intervening particles, scattering by intervening particles (treated individually), and diffraction of part of the radiation as it passes through the gaps between particles. The present theory, being a geometrical-optics approximation, includes only the first two mechanisms. If diffraction contributes a small, but not insignificant, amount to the radiative attenuation, the geometrical optics approximation will tend to become invalid, mutual particle shadowing will be reduced, and a_2 will fall below its geometrical value given by equation (6). If, on the other hand, the diffraction is strong enough to divert radiation from the cylinders of incidence and emission and, thus, add to the effective coefficients of scattering and absorption, a_2 will exceed its geometrical value. Such strong diffraction can occur for sufficiently packed particulate materials and for sufficiently long wavelengths because the interparticle gaps through which the radiation passes can be made much smaller than the particles themselves. The implicit assumption, of course, is that the simple theory herein described can be made to include diffraction effects by the relaxation of the purely geometrical requirements on a_2 and also the geometrical optics restrictions enumerated in reference 3. The subsequent agreement of the theory with experimental data tends to confirm this assumption.

The second reservation concerns the behavior of equation (5) for large angles of incidence or emission. That the analysis in reference 3 is somehow inadequate and not generally valid is evident from the limit (see appendix A)

$$f(i \text{ or } \epsilon = \pi/2; a_2 \neq 0) = 0 \quad (9)$$

This result is clearly nonphysical because under no circumstances should f be less than unity and thereby reduce the reflected intensity below its classical value given by equation (3). In fact, the entire purpose of the shadowing correction of reference 3 was to reduce the attenuation of radiation within the material (and thus increase the emerging intensity) by counting the scattering and absorption of a light beam only in the incident leg of its total path through the volume v' shared by the cylinders of incidence and emission.

Since the improper limit of equation (5) occurs at grazing incidence or emission, it will not significantly affect the determination of the photometric parameters in the present analysis because the experimental data are confined to angles of incidence and emission of 75° or less. However, to avoid most of the error caused by equation (5) for computations carried to large angles of incidence or emission, the following straightforward procedure is suggested and will be used for all subsequent calculations: use equation (5) for

all scattering geometries for which f exceeds unity and replace equation (5) with $f = 1$ for larger values of i or ϵ . This approach might seem crude, as opposed to undertaking a detailed theoretical modification to the equations of reference 3, but the subsequent analysis will show that the aforementioned correction is adequate. Equations (4) to (8), together with the aforementioned procedure for correcting equation (5), thus represent the low-albedo limit to be used in the remainder of this analysis.

Two other important limits of f that will be useful in the subsequent analysis are the following:

$$f(a_2 \equiv 0) = 1 \tag{10}$$

for all values of α , which is the classical result for zero ratio of particle size to mean free photon path, and

$$f(\alpha = 0; a_2 \neq 0) = 2 \tag{11}$$

which corresponds to the well-known opposition effect. (See ref. 5.)

High-Albedo Limit

For reasons covered in the "Introduction," especially with regard to the possibility of important inconsistencies in the method proposed by reference 3 for including higher scattering orders, no attempt will be made to apply ab initio techniques to problems involving multiple scattering. Instead, the intensity in the high-albedo limit of very large multiple scattering is assumed to satisfy the Lambert formula

$$I = C \cos i \tag{12}$$

which corresponds to the complete directional randomization of the incident radiation by a multitude of scattering events.

No theoretical derivation of equation (12) exists from first principles. However, its use can be justified under certain conditions by comparisons with Chandrasekhar's calculations (ref. 2, p. 147) of the diffuse reflection from semi-infinite atmospheres comprised of isotropic or Rayleigh scatterers. He found that for a fixed incident angle and sufficiently large phase angle, the single-scattering contribution to the brightness increases with phase angle, whereas the total brightness computed from all levels of multiple scattering tends to decrease with phase angle. The first of these effects is evident from equation (4) without the f -factor, and the second follows from the fact that multiple scattering, which enhances the brightness, increases with the depth below the atmospheric

surface. Since the depth of the contributing particles decreases with increasing phase angle because of attenuation within the atmosphere, emerging radiation that has been multiply scattered falls off and thus the brightness diminishes. The photometries of bright planetary surfaces, on the other hand, should behave somewhat differently than those of atmospheres because of the far greater particle densities involved. Large multiple scattering occurs in this case within a few particle diameters below the surface; hence, the aforementioned depth-attenuation effect should be much less significant so that the brightness will be relatively insensitive to variations in the phase angle. In addition to these theoretical arguments, support for the use of the Lambert formula in the limit of high albedo is obtained from reference 5 which reports measurements on a bright, heavily smoked MgO surface that are consistent with the Lambert formula.

Photometric Function

The diffuse radiative reflection by a semi-infinite particulate material of any given albedo is assumed to be adequately described by the following linear combination of equations (4) and (12):

$$I(i, \epsilon, \alpha) = C_1 \frac{p(\alpha) f(i, \epsilon, \alpha, a_2) \cos i}{\cos i + \cos \epsilon} + C_2 \cos i \quad (13)$$

where C_1 and C_2 are proportional to the weight factors for the two extremes of single scattering and high-order multiple scattering. Expressions of this form, with f either being unity or the Hapke (ref. 6) shadowing-correction factor, as opposed to that of Irvine, have been previously proposed (see ref. 4) but never verified experimentally. With the aid of equation (11) and the introduction of a_1 for the ratio C_2/C_1 , equation (13) can be represented in normalized form (that is, normalized to unity at $i = \epsilon = 0$) by the function

$$\Phi(i, \epsilon, \alpha) = \frac{\cos i}{[p(0) + a_1](\cos i + \cos \epsilon)} \left[p(\alpha) f(i, \epsilon, \alpha, a_2) + a_1(\cos i + \cos \epsilon) \right] \quad (14)$$

The parameter a_1 is thus a measure of the multiple scattering occurring in the particulate material and therefore relates to the single-particle albedo. Its value ranges from zero for very dark materials to infinity for Lambert surfaces.

Except for the specification of the phase function $p(\alpha)$, the formulation of the photometric function is now complete. For the purposes of the present analysis, the phase function

$$p(\alpha) = 1 + a_0 \cos \alpha \quad (15)$$

will be used because it qualitatively describes the entire range of simple scattering laws from predominantly forward scatter for $-1 \leq a_0 < 0$ (for example, transmission through small particles) to predominantly backscatter for $0 < a_0 \leq 1$, including isotropic scattering at $a_0 = 0$. Accordingly, equation (14) becomes

$$\Phi(i, \epsilon, \alpha) = \frac{\cos i}{(1 + a_0 + a_1)(\cos i + \cos \epsilon)} \left[(1 + a_0 \cos \alpha) f(i, \epsilon, \alpha, a_2) + a_1(\cos i + \cos \epsilon) \right] \quad (16)$$

Equation (16) is thus the complete form of the photometric function proposed for use in the analysis of diffuse reflection from particulate materials. The reader is cautioned that f must be corrected according to the discussion following equation (9).

Although the linear combination of terms in equation (16) was not derived from first principles, it will be seen in subsequent sections to be in good quantitative agreement with experimental brightness data. Moreover, variations in the physical properties of laboratory surfaces will be shown to cause changes in the parameters a_0 , a_1 , and a_2 that are consistent with their theoretical interpretations; thus, the determination of these parameters from fits of equation (16) to photometric measurements should yield valuable information on surface characteristics. It is instructive, however, first to consider some of the implications of equation (16) pertaining to the familiar Minnaert function (ref. 1) and to the prediction of several well-known planetary photometric phenomena.

The Minnaert function

$$\Phi(i, \epsilon, \alpha) = B(\alpha) (\cos i)^{k(\alpha)} (\cos \epsilon)^{k(\alpha)-1} \quad (17)$$

is shown in appendix B to be in good agreement with equation (16) for variations of i and ϵ with α held fixed and coincident planes of incidence and emission, provided the deviation from the mirror-point geometry (that is, equal incident and emission angles on opposite sides of the surface normal) is not too large. This class of scattering geometries is especially important because the Minnaert function is known to represent adequately the photometries of at least the surfaces of Mars and of the Moon for such conditions (for example, refs. 7, 8, and 9 on photometric measurements of Mars).

The implications of equations (13) and (14) at zero phase angle can also be studied. By using equations (10) and (11) and the relation $a_1 = C_2/C_1$ in equation (13), one obtains

$$\frac{I(i = \epsilon; a_2 \neq 0)}{I(i = \epsilon; a_2 = 0)} = \frac{2[p(0) + a_1 \cos i]}{p(0) + 2a_1 \cos i} \quad (18)$$

An immediately obvious conclusion is that low planetary albedos (small a_1) are correlated with large opposition effects, as was found by Thompson (ref. 10) and as should be expected on the basis that the particle-shadowing origin of the opposition effect can be dominant only in the single-scattering contribution and should rapidly diminish as the level of multiple scattering increases. A second result follows from

$$\Phi'(i = \epsilon; \text{small } a_1; a_2 = 0) \approx 1 - \frac{2a_1}{p(0)}(1 - \cos i) \quad (19)$$

which is the first-order expansion in a_1 of the normalized (no shadowing) brightness

$$\Phi'(i, \epsilon, \alpha; a_2 = 0) = \frac{2 \cos i}{[p(0) + 2a_1](\cos i + \cos \epsilon)} [p(\alpha) + a_1 (\cos i + \cos \epsilon)] \quad (20)$$

obtained from equations (10) and (13), and the following expansion of equation (14):

$$\Phi(i = \epsilon; \text{small } a_1; a_2 \neq 0) \approx 1 - \frac{a_1}{p(0)}(1 - \cos i) \quad (21)$$

Equation (19) (no shadowing) and equation (21) (shadowing) indicate that a low albedo (small a_1) generally means a small amount of planetary limb darkening. The reduced sensitivity to i of equation (21) means even less limb darkening when shadowing is present. One notes that the moon is relatively dark, has a strong opposition effect due to shadowing, and displays practically no limb darkening. (See ref. 6.)

PHOTOMETRIC MEASUREMENTS

Laboratory brightness measurements were made to provide support in the development and the verification of the photometric function. Photometric data were taken on two materials: a Colorado basalt and a basalt dune sand. The Colorado basalt is a mafic latite porphyry from an area in the vicinity of the Ralston intrusives and the Table Mountain region of Colorado; the basalt dune sand is believed to have originated from the airfall cinder sheet deposited in the eruption of Sunset Crater and transported by aeolian processes to an area of active dunes 25 km east of Flagstaff, Arizona. The basalts have properties that may be similar to those of the Martian surface material and they have silicon-dioxide contents within the range measured by the infrared spectroscopy experiment on Mariner 9 as being representative of the content of the Martian dust. (See ref. 11.) The latite was mechanically crushed to small sizes, but the dune sand was used unaltered.

Each material was mechanically sieved into two particle-size ranges; figure 1 gives the particle size distributions of the test materials. Loosely packed, optically thick test surfaces were formed by sifting the particles upon flat base layers of the same material. The surfaces were contained within a 1.5-m-diameter pan and were illuminated by parallel light from a high-pressure, short-arc mercury lamp at the focal point of a 61-cm-diameter parabolic mirror. Reflected light was measured with a silicon-diffused photodiode at the focal point of a second 61-cm-diameter parabolic mirror. Both mirrors are movable along a semicircular guide 3.7 m in diameter. Figure 2 is a photograph of the photometric apparatus. Although the use of large mirrors prohibits measurements at small phase angles (in this case smaller than 30°) and results in a definite disadvantage for the present purposes, the large illuminated areas permit possible future studies of the photometric effects of rough surface topographies which are more difficult to represent on a smaller scale.

Photometric data for coplanar scattering geometries were taken as the two mirrors were moved in unison (2.5° steps) along the supporting guide and thereby the angles of incidence and emission were changed while the phase angle was held constant. Sets of measurements on each of the four laboratory materials (namely, two particle-size ranges for each of the basalts) were obtained in this manner for eleven values of the phase angle from 30° to 80° in 5° steps.

DATA ANALYSIS

The determination of the three photometric parameters a_0 , a_1 , and a_2 was accomplished by comparing equation (16) with brightness measurements for two classes of scattering geometries: variations of i and ϵ with α held constant and variations in α with ϵ fixed at 0° . All measurements were restricted to coincident planes of incidence and emission. An iterative procedure was followed that involved choices of the parameters until the brightnesses computed from equation (16) were in satisfactory agreement with the experimental data. The results are given in table I for the four laboratory materials. Comparisons between theory and experiment are shown in figures 3 and 4 in two forms: as plots of the effective Minnaert exponent $k(\alpha)$ in figures 3(a) and 3(b) for the first class of geometries and as plots of the normalized brightness Φ in figures 4(a) and 4(b) for the second class.

As discussed in appendix B, Minnaert plots of the brightness for the first class of geometries are nearly linear with slopes equal both to the $k(\alpha)$ -exponent in equation (17) and to the appropriate approximation (also discussed in appendix B) to the logarithmic derivative of equation (16). The $k(\alpha)$ exponent contains the complete dependence of the brightness on a_0 , a_1 , and a_2 for these geometries; moreover, the specification of k

TABLE I.- EMPIRICAL PARAMETERS FOR LABORATORY MATERIALS

Material	Mean particle diameter, μm	a_0	a_1	a_2
Colorado basalt (latite)	105	-0.40	0.28	0.32
Colorado basalt (latite)	225	-.10	.26	.15
Basalt dune sand	125	-.10	.25	.17
Basalt dune sand	210	.05	.20	.09

over the experimental range of α provides a convenient and concise method for representing the most important content of the numerous brightness measurements employed in this case. Accordingly, the variation of k with α , rather than the variation of Φ with angles, was chosen as the mode of comparison between theory and experiment in figure 3.

The comparisons shown in figures 3 and 4 indicate that for at least two different classes of geometries, equation (16) adequately describes the photometric behavior of the four laboratory samples, at least over the range of phase angle that was used in the experiments. The noticeable but insignificant discontinuities in the slopes of the brightnesses at large phase angles in figure 4 are the result of the correction to equation (5). Such discontinuities are to be expected at the points where the f of equation (5) is replaced by $f = 1$ according to the procedure discussed after equation (9). Since, however, these two classes of geometries were used in the determination of the values of the three parameters, additional comparisons for other geometries are desirable. Accordingly, the same values of the photometric parameters were used with equation (16) for coincident-plane variations of ϵ , i being fixed first at 45° and then at 60° . The results are shown in figures 5 to 7; they are in very good agreement with experimental data over the range in which comparisons can be made. This agreement indicates that equation (16) and the values of the photometric parameters in table I are not restricted to the previous scattering conditions. As previously explained, the limitations of the experimental apparatus prevented measurements in the vicinity of $\alpha = 0$ (the opposition effect), where pronounced cusps occur in figures 5 to 7. Verification of the applicability of equation (16) to other scattering geometries and, in particular, to scattering geometries corresponding to noncoincident planes of incidence and emission has been obtained by Daniel J. Jobson (presented in part in ref. 12) in brightness measurements on the Colorado basalt of $225 \mu\text{m}$ mean particle diameter.

Also shown in figure 5 is a dashed curve that was computed by use of the f of equation (5) over the entire range of ϵ , without the aforementioned correction for the

nonphysical behavior of that expression at large i or e . It is evident that the correction is important and that a straightforward application of the analysis in reference 3 can result in a significant underestimate of the brightness at grazing incidence or emission. Figure 5 was chosen to illustrate these errors because the laboratory sample it represents yields the largest experimentally determined value of a_2 , which corresponds to the largest errors caused by the deficiencies in equation (5).

Some additional support for the validity of equation (16) and, more importantly, some confidence in the general application of the photometric function can be obtained from reference 13 which presents brightness data for such diverse scattering surfaces as beach sand, black loam, and green grass. These data exhibit a remarkable similarity to the plot of equation (16) in figures 5 to 7 in three respects: a pronounced cusp at $\alpha = 0$, an increasing trend in brightness to the left and to the far right of the graph, and a broad minimum in between. (Ref. 13 does not present sufficient data for the three photometric parameters of eq. (16) to be determined for the substances studied in that reference.)

INTERPRETATION OF PHOTOMETRIC PARAMETERS

In addition to the good quantitative agreement between experimental data and the surface brightnesses predicted by equation (16), the validity of the proposed photometric function is further substantiated by the changes in the empirical parameters a_0 , a_1 , and a_2 as the mean particle size is altered for a given material. For example, the phase-function parameter a_0 is more negative in table I for the small particle sizes of each material; thereby enhanced transmission through individual particles is suggested. The same enhanced transmission is also displayed in figures 5 to 7, where the brightness at large phase angles to the left in each figure is always higher (at a fixed value of i) for the smaller particles than for the larger ones.

The parameter a_1 measures the amount of multiple scattering and thus relates to the single-particle albedo. In table I, a_1 increases for both materials as the particle size decreases; hence, some of the radiation that would be absorbed by the larger particles is transmitted through the smaller ones to be scattered again and partially to emerge as reflected light. This interpretation is consistent with the observation that, for sufficiently small particles, surfaces generally become brighter as the particle size is diminished.

Finally, the packing factor a_2 increases with decreasing particle size (table I) to imply a less porous structure for the small-particle surfaces and correspondingly smaller opposition effects, which are seen in figure 4 as a smaller rate of change in the slope of Φ as the phase angle approaches zero. Such behavior of a_2 may be the result of the smaller apertures between the particles of the small-particle samples; these smaller apertures could cause greater diffraction of the light passing through these apertures and

thus correspond to an increase in the apparent packing of the surface as deduced from photometry. As mentioned previously in the discussion after equation (8), diffraction probably causes ρ to exceed the mean particle radius and thereby increases the value of a_2 . The fact that three of the four values of a_2 in table I exceed the upper limit 0.125 imposed by a strict geometric interpretation of ρ as the mean particle radius and corresponding to $\rho = 0.5n^{-1/3}$ might be regarded as support for the importance of strong diffraction. Brightness measurements with some wavelength discrimination are obviously desirable to provide additional information on this point because diffraction would cause a_2 to increase with increasing wavelength.

CONCLUDING REMARKS

A photometric function has been proposed that appears to give reliable descriptions of the diffuse reflection of radiation by particulate materials. It was designed to yield accurate results in the opposing limits of very low albedo and very high levels of multiple scattering and has been shown to be in satisfactory agreement with laboratory measurements on materials lying between these two extremes. Small discrepancies between theory and experiment at large angles of incidence or emission are explained in terms of the approximations made in the shadowing corrections to the classical theory of radiative transfer.

The function is applicable to such problems as the extrapolation of planetary brightness measurements over wide ranges of scattering geometries. It can also be applied to the deduction of compactness, particle size, and single-particle albedo of planetary surfaces by the evaluation of the empirical parameters in the function. Observed changes in these parameters with changes in the laboratory samples have been shown to be consistent with the theoretical interpretations, and this consistency furnishes evidence of the validity of the proposed function. Future research in this field should include spectral determinations of the photometric parameters a_0 , a_1 , and a_2 . All these parameters are expected to be functions of the wavelength because of diffraction effects. A verification of the predicted wavelength dependence will lend additional support to the theory and aid in the deduction of surface properties from photometric measurements.

Langley Research Center,
National Aeronautics and Space Administration,
Hampton, Va., February 5, 1975.

APPENDIX A

DERIVATION OF SHADOWING-CORRECTION FACTOR FOR SINGLE SCATTERING

The purpose of this appendix is to define the shadowing-correction factor f and to derive its form for general scattering geometries. The development generally follows that of reference 3 which does not explicitly define a shadowing-correction factor and uses substantially different notation. This appendix also shows explicitly how the shadowing-correction factor becomes invalid for grazing angles of incidence or emission and suggests a simple procedure for correcting the deficiency.

Figure 8 shows the scattering geometry for a beam of radiation incident on a particle located at the origin of the ξ, η, z coordinate system. The beam is scattered into the direction of the ξ -axis and the coordinate system is oriented so that the ξ, η -plane coincides with the scattering plane. (That is, the ξ, η -plane contains the beams of incidence and emission.) The plane shown cutting the coordinate system represents the surface of the reflecting material and lies at the perpendicular distance h above the scattering particle. In addition to the angle of incidence i , the angle of emission ϵ , and the phase angle α between the incident and emitted beams, a fourth angle γ is introduced as the angle between the η -axis and the projection of h onto the η, z -plane. Useful expressions that can be obtained directly from figure 8 are the equation for γ as a function of i , ϵ , and α and the equation for the plane of the surface. These expressions are

$$\gamma = \cos^{-1} \left(\frac{\cos i - \cos \epsilon \cos \alpha}{\sin \epsilon \sin \alpha} \right) \quad (A1)$$

and

$$\xi \cos \epsilon + \eta \sin \epsilon \cos \gamma = h - z \sin \epsilon \sin \gamma \quad (A2)$$

According to the principles of geometrical optics and with the restriction to single scattering, an incident photon will reach the scattering particle in figure 8, will be scattered, and will emerge from the material only if no particle center lies within the volume enclosed by two imaginary cylinders (radii equal to the average particle radius ρ) extending from the scattering particle to the surface along the directions of incidence and emission. The probability for no particle center to lie within this volume is given by the expression

APPENDIX A

$$P = \left(1 - \frac{v - v'}{V}\right)^N \approx 1 - n(v - v') \approx \exp[-n(v - v')] \quad (\text{A3})$$

where $n = N/V$ is the number density of particles comprising the particulate material, v is the sum of the volumes of the cylinders of incidence and emission, and v' is the overlap volume between these two cylinders that must be subtracted from v in order not to be counted twice.

If, on the other hand, the particles are sufficiently separated that each particle is in the far field for scattering by every other particle, the geometrical optics approximation breaks down, shadowing fails to occur, and the overlap volume v' should be counted twice in computing the total attenuation of the incident and emitted beam. The probability P for this latter case, as opposed to the P in equation (A3) for planetary surfaces, yields the Chandrasekhar result for atmospheres that appears in equation (3). Hence, the shadowing-correction factor f to the first-order solution of Chandrasekhar's radiative transfer equation can be defined as follows for a semi-infinite particulate material:

$$f = \frac{\int_0^\infty \exp[-n(v - v')] dh}{\int_0^\infty \exp(-nv) dh} = \frac{\pi n \rho^2 (\cos i + \cos \epsilon)}{\cos i \cos \epsilon} \int_0^\infty \exp[-n(v - v')] dh \quad (\text{A4})$$

Figure 9 shows the intersections with the plane $z = z$ in figure 8 of the material surface (line (1)), the cylinder of incidence, and the cylinder of emission. The equation for line (1) is given by equation (A2) and the equations for lines (2) and (3) are

$$\eta = (\rho^2 - z^2)^{1/2} \quad (\text{A5})$$

and

$$\xi \sin \alpha - \eta \cos \alpha = (\rho^2 - z^2)^{1/2} \quad (\text{A6})$$

respectively. If line (1) is ignored for the moment, the overlap area A' common to both cylinders is

$$A' = \frac{(\rho^2 - z^2)(1 + \cos \alpha)}{\sin \alpha} \quad (\text{A7})$$

APPENDIX A

so that the total overlap volume V' of the two cylinders can be written

$$V' = 2 \int_0^{\rho} A' dz = \frac{4\rho^3(1 + \cos \alpha)}{3 \sin \alpha} \equiv \frac{\mu}{n} \quad (\text{A8})$$

The volume V' in equation (A8) is to be equated to the volume v' in equation (A4) for all particles so that the overlap volume of the two cylinders is entirely contained within the scattering medium. For particles lying closer to the surface, the area A'' bounded by lines (1), (2), and (3) in figure 9 and given by the following expression must be considered:

$$\begin{aligned} A'' &= \frac{1}{\sin \alpha \cos \epsilon} \int_{\eta_1}^{(\rho^2 - z^2)^{1/2}} \left[(\rho^2 - z^2)^{1/2} \cos \epsilon - h \sin \alpha + z \sin \alpha \sin \epsilon \sin \gamma \right. \\ &\quad \left. + \eta(\cos \alpha \cos \epsilon + \sin \alpha \sin \epsilon \cos \gamma) \right] d\eta \\ &= \frac{(\cos i + \cos \epsilon)^2}{2 \sin \alpha \cos i \cos \epsilon} \left[(\rho^2 - z^2)^{1/2} - \rho x (1 + g^2)^{1/2} + gz \right]^2 \end{aligned} \quad (\text{A9})$$

Equation (A1) and the definition

$$x = \frac{h \sin \alpha}{\rho(\cos i + \cos \epsilon)(1 + g^2)^{1/2}} \quad (\text{A10})$$

where

$$g = \frac{\sin \alpha \sin \epsilon \sin \gamma}{\cos i + \cos \epsilon} \quad (\text{A11})$$

have been used in the evaluation of the integral, the lower limit η_1 of which corresponds to the null integrand.

The area A'' is zero when

$$z = z_1 = \rho (1 + g^2)^{-1/2} \left[gx - (1 - x^2)^{1/2} \right] \quad (\text{A12})$$

APPENDIX A

and

$$z = z_2 = \rho(1 + g^2)^{-1/2} \left[gx + (1 - x^2)^{1/2} \right] \quad (\text{A13})$$

which values appear as integration limits in the formula

$$v'' = \int_{z_1}^{z_2} A'' dz = \frac{\nu}{6\pi n} \left[2(2 + x^2)(1 - x^2)^{1/2} - 3x(\pi - 2 \sin^{-1} x) \right] \quad (\text{A14})$$

for that part of the overlap volume situated outside the scattering medium. The new parameter ν is defined by the relation

$$\begin{aligned} \nu &= \frac{\pi n \rho^3 (1 + g^2)^{1/2} (\cos i + \cos \epsilon)^2}{\sin \alpha \cos i \cos \epsilon} \\ &= \frac{\pi n \rho^3 (\cos i + \cos \epsilon)}{\sin \alpha \cos i \cos \epsilon} \left[\sin^2 \alpha + 2(1 + \cos \alpha) \cos i \cos \epsilon \right]^{1/2} \end{aligned} \quad (\text{A15})$$

Accordingly, the overlap volume contained within the scattering material is given by

$$v' = V' - v'' = \frac{\mu}{n} - v'' = \frac{\mu}{n} - \frac{\nu}{6\pi n} \left[2(2 + x^2)(1 - x^2)^{1/2} - 3x(\pi - 2 \sin^{-1} x) \right] \quad (\text{A16})$$

if the surface intersects the total overlap volume and by

$$v' = \frac{\mu}{n} \quad (\text{A17})$$

if the surface does not intersect the total overlap volume. The dividing line between these two expressions occurs at $x = 1$, which is obtained by setting v'' equal to zero in equation (A14). Although reference 3 uses equation (A16) over the entire range $0 \leq x \leq 1$, the reader should be cautioned that the formula is not valid for particles that are so close to the surface as to cause line (1) in figure 9 to intersect one or both of the bases of the cylinders of incidence and emission. The deficiency is especially important near grazing incidence or emission because surface-layer particles dominate the reflectance in such cases. For example, the limit of the v' in equation (A16) at $x = 0$ and for i or ϵ

APPENDIX A

equal to $\pi/2$ is $-\infty$; this limit causes the shadowing-correction factor f defined by equation (A4) to vanish. The correct expression for f can never be less than unity because shadowing only operates to decrease the attenuation of the radiation and thus to increase the surface brightness.

The substitution into equation (A4) of equations (A16) and (A17) and the formula

$$v = \pi \rho^2 h \left(\frac{1}{\cos i} + \frac{1}{\cos \epsilon} \right) \quad (\text{A18})$$

for the sum of the volumes of the cylinders of incidence and emission (corresponding to a particle that is sufficiently deep for the surface of the material not to intersect the base of either cylinder) yields

$$f = e^{\mu - \nu} + \nu \int_0^1 \exp \left\{ \mu - \frac{\nu}{6\pi} \left[2(2 + x^2)(1 - x^2)^{1/2} + 3x(\pi + 2 \sin^{-1} x) \right] \right\} dx \quad (\text{A19})$$

for the shadowing-correction factor of reference 3. Equation (A19) and equations (A8) and (A15) for μ and ν , respectively, also specify the shadowing correction employed in the present research, but with the important exception that f is replaced by unity whenever equation (A19) gives f below that value. This rather crude, but experimentally justified, procedure for correcting the aforementioned deficiency near grazing angles of incidence or emission is introduced because of a fundamental difficulty associated with the extension of the geometrical cylinder concept to surface-layer particles. The value of ν given by equation (A18) occurs in the exact solution (see eq. (3)) of Chandrasekhar's first-order radiative transfer equation for all values of x , including $x = 0$, even though equation (A18) is not the true sum of the cylinder volumes for sufficiently small x .

APPENDIX B

COMPARISON WITH MINNAERT'S FUNCTION

Because the Minnaert photometric function of equation (17) is the analytic form almost invariably used to correlate measured brightness data regardless of the scattering geometry, a comparison of it with the photometric function developed in this paper is important. Minnaert's function is a simple empirical generalization of Lambert's law and has very insufficient basis in theory. It has been used successfully, however, to correlate brightness measurements of the Martian surface. (See refs. 7, 8, and 9.) The measurements were made for the special class of scattering geometries corresponding to coincident plane variations in i and ϵ with the phase angle α held fixed. They yielded approximately linear curves in so-called Minnaert plots of $\log(\Phi \cos \epsilon)$ plotted against $\log(\cos i \cos \epsilon)$ at constant α ; this behavior is predicted by equation (17). Seldom, though, have the measurements been extended to very large departures from the mirror-point geometry (that is, equal incident and emission angles on opposite sides of the surface normal) or to large phase angles (for example, $\alpha \approx 22^\circ$ in Mariner 6 and 7 far-encounter data and $\alpha \leq 18.5^\circ$ for the Earth-based measurements of Binder and Jones (ref. 8)); therefore, nonlinear portions of Minnaert plots may well exist without contradicting the available experimental evidence.

Some basic insight into the characteristics of Minnaert plots of equation (14) may be gained by looking at the Lommel-Seeliger limit of Φ as a_1 and a_2 approach zero and f approaches unity. The conclusions should be qualitatively general because the shadowing-correction factor f should exert a major influence only near zero phase angle and the Lambert term corresponds to a linear Minnaert plot of slope unity. The differentiation (for fixed α) with respect to $\log_e(\cos i \cos \epsilon)$ of the natural logarithm of the expression

$$\Phi(\text{Lommel-Seeliger}) \cos \epsilon = \frac{2p(\alpha) \cos i \cos \epsilon}{p(0)(\cos i + \cos \epsilon)} \quad (\text{B1})$$

is required.

If the angular deviation δ from the mirror-point geometry is defined by the expression

$$\delta = i - \frac{\alpha}{2} = \frac{\alpha}{2} - \epsilon \quad (\text{B2})$$

APPENDIX B

the following relations are valid through low-order expansions in δ :

$$\cos i \cos \epsilon = \cos^2 \frac{\alpha}{2} - \delta^2 + \frac{\delta^4}{3} \quad (\text{B3})$$

$$\cos i + \cos \epsilon = \left(2 - \delta^2 + \frac{\delta^4}{12} \right) \cos \frac{\alpha}{2} \quad (\text{B4})$$

and

$$\frac{d}{d(\log_e \cos i \cos \epsilon)} = -\cos^2 \frac{\alpha}{2} \left(1 + \frac{2\delta^2}{3} - \frac{\delta^2}{\cos^2 \frac{\alpha}{2}} \right) \frac{d}{d(\delta^2)} \quad (\text{B5})$$

Hence, the Minnaert-plot slope of equation (B1) is given by

$$\begin{aligned} \text{Slope} &= \frac{d}{d(\log_e \cos i \cos \epsilon)} \left[\log_e \left(\frac{\cos i \cos \epsilon}{\cos i + \cos \epsilon} \right) \right] \\ &\approx 1 + \frac{\cos^3 \frac{\alpha}{2}}{\cos i + \cos \epsilon} \left(1 + \frac{2\delta^2}{3} - \frac{\delta^2}{\cos^2 \frac{\alpha}{2}} \right) \frac{d}{d(\delta^2)} \left(2 - \delta^2 + \frac{\delta^4}{12} \right) \\ &\approx 1 - \frac{1}{2} \cos^2 \frac{\alpha}{2} + \frac{\delta^2}{2} \sin^2 \frac{\alpha}{2} \end{aligned} \quad (\text{B6})$$

If the first two terms in equation (B6) are identified with the Minnaert exponent $k(\alpha)$ in equation (17), the Lommel-Seeliger function (and thus the proposed function as well) is accurately approximated by a Minnaert function over a significant range of δ , especially for small α ; hence, equation (14) is consistent with the limited planetary data for this particular class of scattering geometries. Equation (B6) also predicts increases in Minnaert-plot slopes for sufficiently large values of δ (that is, small values of $\cos i \cos \epsilon$). Direct experimental evidence of such behavior is shown in figure 10, where a typical set of brightness data points for one of the laboratory materials is plotted in Minnaert coordinates. The measured values are shown as solid circles, a straight line being shown for comparison. The trend toward greater slopes as δ increases to the left in the figure is typical of the test surfaces. Also typical is the linear section of the curve extending for some distance from the mirror point which is at the right-hand end of the

APPENDIX B

curve, where $\delta = 0$. The slight deviation from linearity in the immediate neighborhood of the mirror point is attributable to the experimental apparatus.

The constant part of the slope of a Minnaert plot of equation (16) is obtained from the equation

$$k(\alpha) = \lim_{\delta \rightarrow 0} \left\{ \frac{d[\log_e (\Phi \cos \epsilon)]}{d[\log_e (\cos i \cos \epsilon)]} \right\}_{\alpha = \text{Constant}} \quad (\text{B7})$$

and is given by

$$k(\alpha) \approx 1 - \frac{1}{2} \cos^2 \frac{\alpha}{2} - \frac{p(\alpha) H(\alpha) - a_1 \cos(\alpha/2)}{p(\alpha) G(\alpha) + 2a_1 \cos(\alpha/2)} \cos^2(\alpha/2) \quad (\text{B8})$$

where

$$H(\alpha) = \frac{4\pi a_2 \tan^2(\alpha/2)}{\sin \alpha} \left\{ J_1(\alpha) - \exp \left[\frac{4a_2(1 - 3\pi + \cos \alpha)}{3 \sin \alpha} \right] \right\} \quad (\text{B9})$$

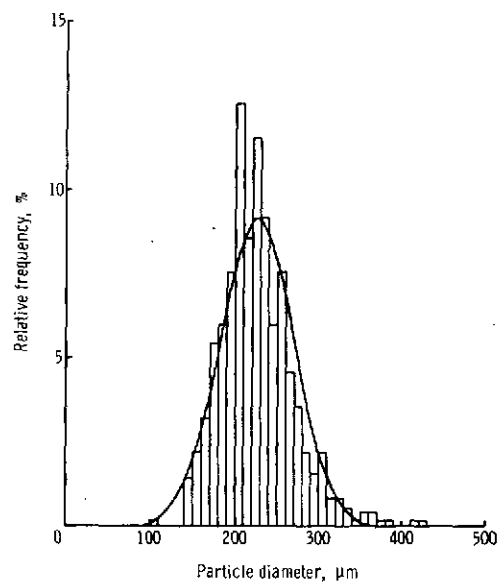
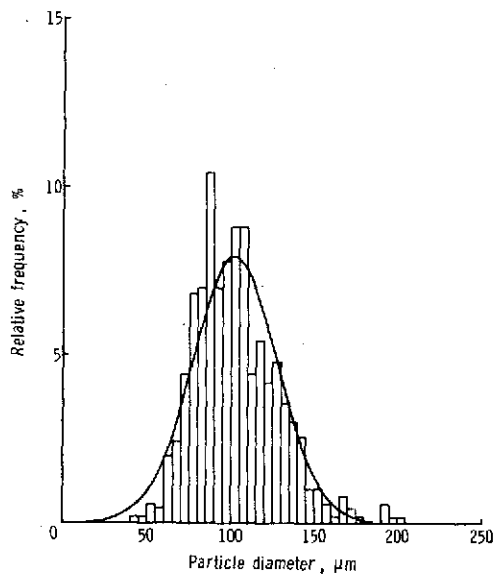
$$G(\alpha) = \frac{4\pi a_2}{\sin \alpha} J_2(\alpha) + \exp \left[\frac{4a_2(1 - 3\pi + \cos \alpha)}{3 \sin \alpha} \right] \quad (\text{B10})$$

$$J_1(\alpha) = J_2(\alpha) - \frac{2a_2}{3 \sin \alpha} \int_0^1 \left[3\pi x + 6x \sin^{-1} x + 2(2 + x^2)(1 - x^2)^{1/2} \right] \\ \times \exp \left\{ \frac{2a_2}{3 \sin \alpha} \left[2 + 2 \cos \alpha - 3\pi x - 6x \sin^{-1} x - 2(2 + x^2)(1 - x^2)^{1/2} \right] \right\} dx \quad (\text{B11})$$

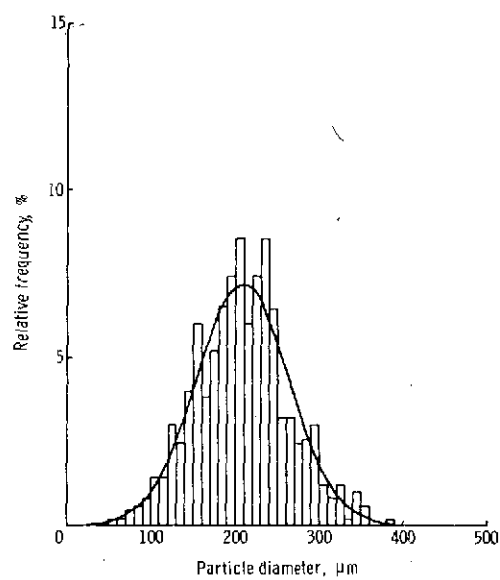
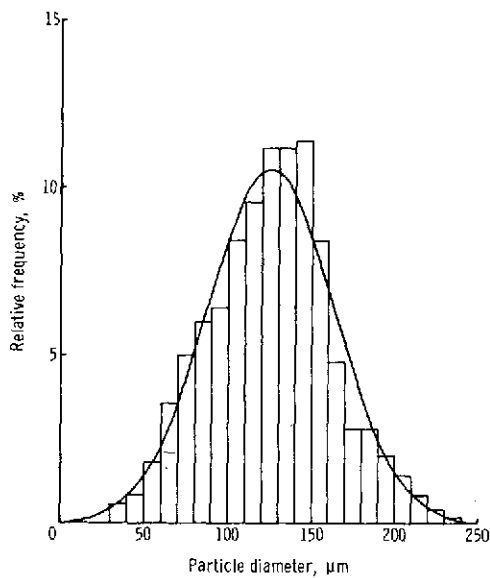
$$J_2(\alpha) = \int_0^1 \exp \left\{ \frac{2a_2}{3 \sin \alpha} \left[2 + 2 \cos \alpha - 3\pi x - 6x \sin^{-1} x - 2(2 + x^2)(1 - x^2)^{1/2} \right] \right\} dx \quad (\text{B12})$$

REFERENCES

1. Minnaert, M.: The Reciprocity Principle in Lunar Photometry. *Astrophys. J.*, vol. 93, no. 3, May 1941, pp. 403-410.
2. Chandrasekhar, S.: *Radiative Transfer*. Dover Pub., Inc., c.1960.
3. Irvine, William M.: The Shadowing Effect in Diffuse Reflection. *J. Geophys. Res.*, vol. 71, no. 12, June 15, 1966, pp. 2931-2937.
4. Aleksandrov, Yu. V.; and Lupishko, D. F.: The Distribution Function of the Normal Albedo of the Surface of Mars. *Solar System Res.*, vol. 6, no. 1, Jan.-Mar. 1972, pp. 7-9.
5. Oetking, Philip: Photometric Studies of Diffusely Reflecting Surfaces With Applications to the Brightness of the Moon. *J. Geophys. Res.*, vol. 71, no. 10, May 15, 1966, pp. 2505-2513.
6. Hapke, Bruce W.: A Theoretical Photometric Function for the Lunar Surface. *J. Geophys. Res.*, vol. 68, no. 15, Aug. 1, 1963, pp. 4571-4586.
7. Young, A. T.; and Collins, S. A.: Photometric Properties of the Mariner Cameras and of Selected Regions on Mars. *J. Geophys. Res.*, vol. 76, no. 2, Jan. 10, 1971, pp. 432-437.
8. Binder, Alan B.; and Jones, J. Colin: Spectrophotometric Studies of the Photometric Function, Composition, and Distribution of the Surface Materials of Mars. *J. Geophys. Res.*, vol. 77, no. 17, June 10, 1972, pp. 3005-3020.
9. Thorpe, Thomas E.: Mariner 9 Photometric Observations of Mars From November 1971 Through March 1972. *ICARUS*, vol. 20, no. 4, Dec. 1973, pp. 482-489.
10. Thompson, Don T.: Time Variation of Martian Regional Contrasts. *ICARUS*, vol. 20, no. 1, Sept. 1973, pp. 42-47.
11. Hanel, R.; Conrath, B.; Hovis, W.; Kunde, V.; Lowman, P.; Maguire, W.; Pearl, J.; Pirraglia, J.; Prabhakara, C.; Schlachman, B.; Levin, G.; Straat, P.; and Burke, T.: Investigation of the Martian Environment by Infrared Spectroscopy on Mariner 9. *ICARUS*, vol. 17, no. 2, Oct. 1972, pp. 423-442.
12. Huck, Friedrich O.; Taylor, Edward J.; Jobson, Daniel J.; and Rowland, Carroll W.: Description and Evaluation of the Viking Lander Camera - Performance Prediction Program. NASA TM X-72646, 1975.
13. Coulson, K. L.; Bouricius, G. M. B.; and Gray, E. L.: Effects of Surface Reflection on Radiation Emerging From the Top of a Planetary Atmosphere. NASA CR-68221, 1966.

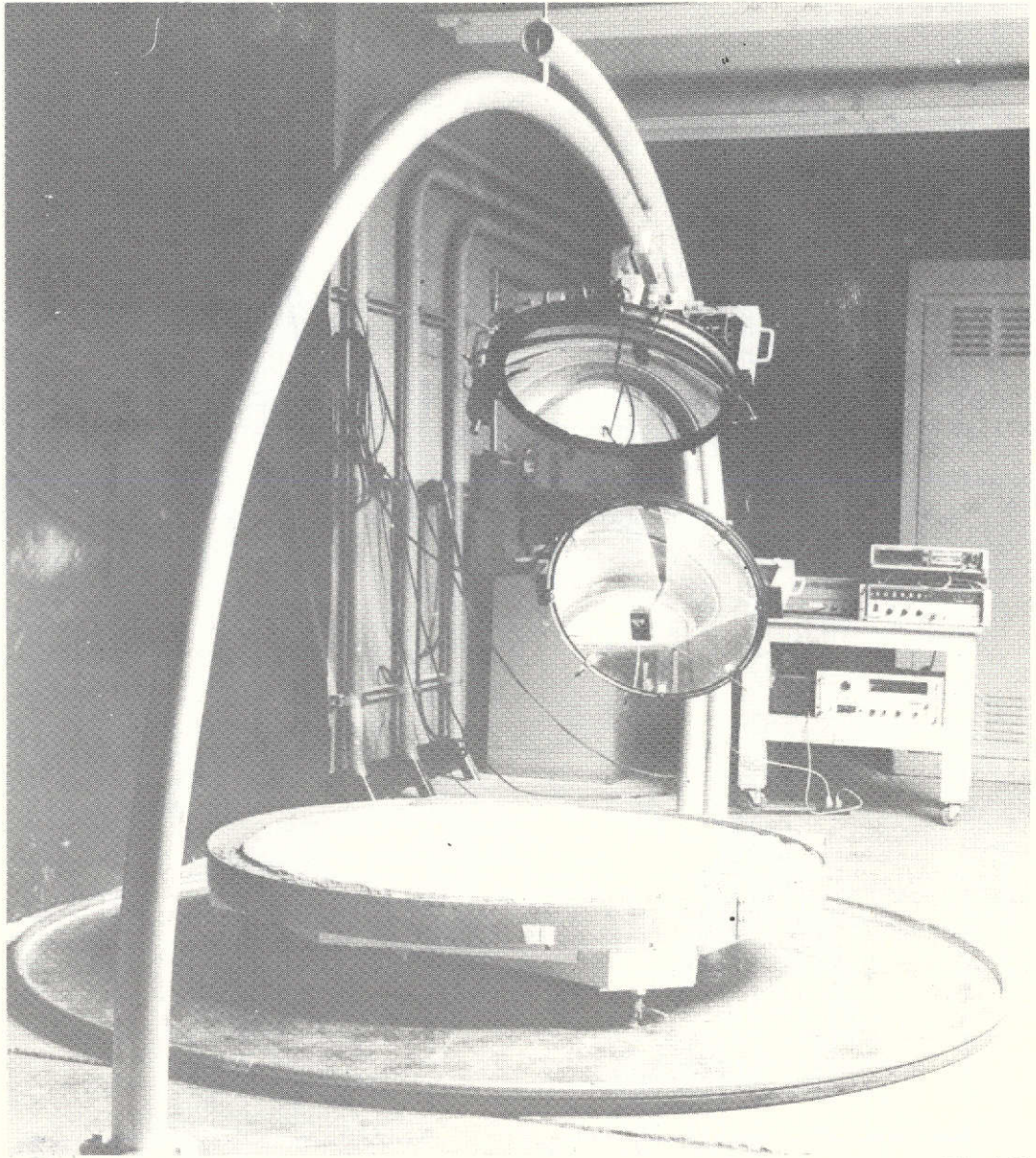


(a) Colorado basalt.



(b) Basalt dune sand.

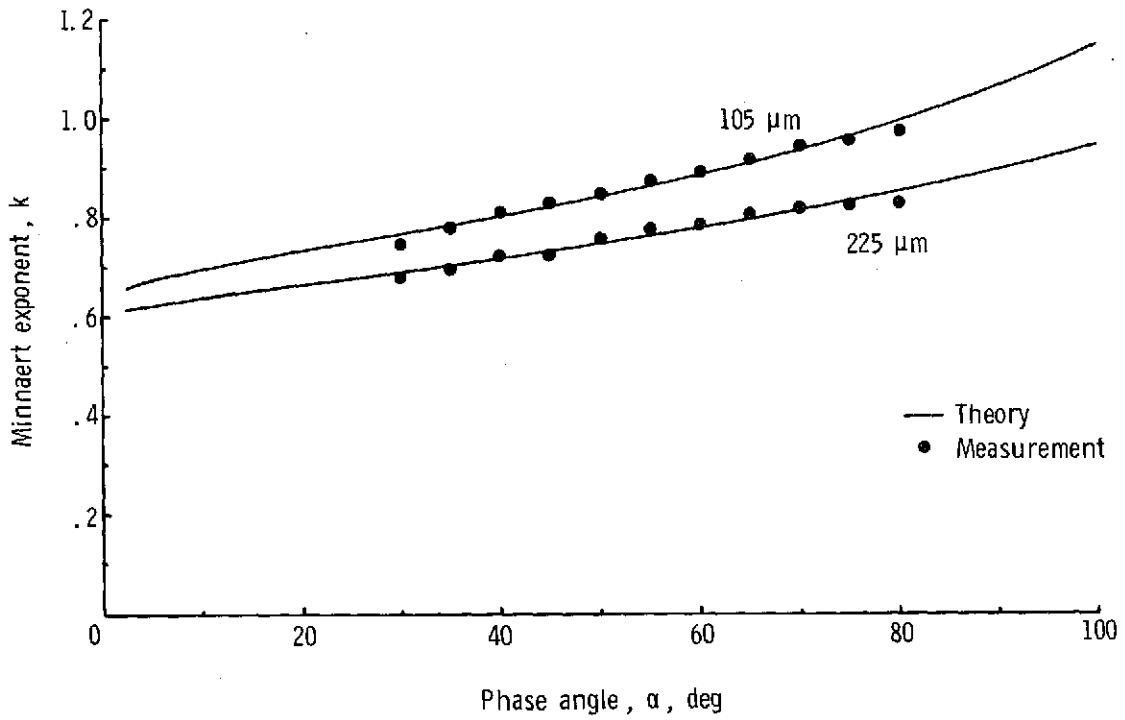
Figure 1.- Relative frequency (number of particles per particle size increment) in percent as function of particle diameter.



L-75-141

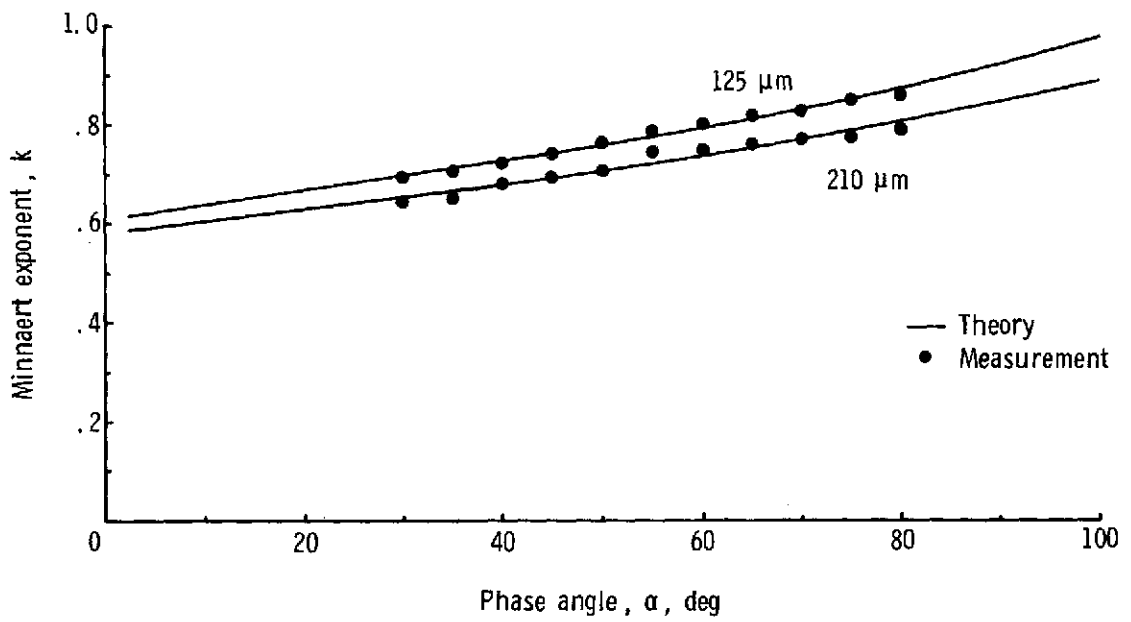
Figure 2.- Photograph of photometric apparatus.

**ORIGINAL PAGE IS
OF POOR QUALITY**



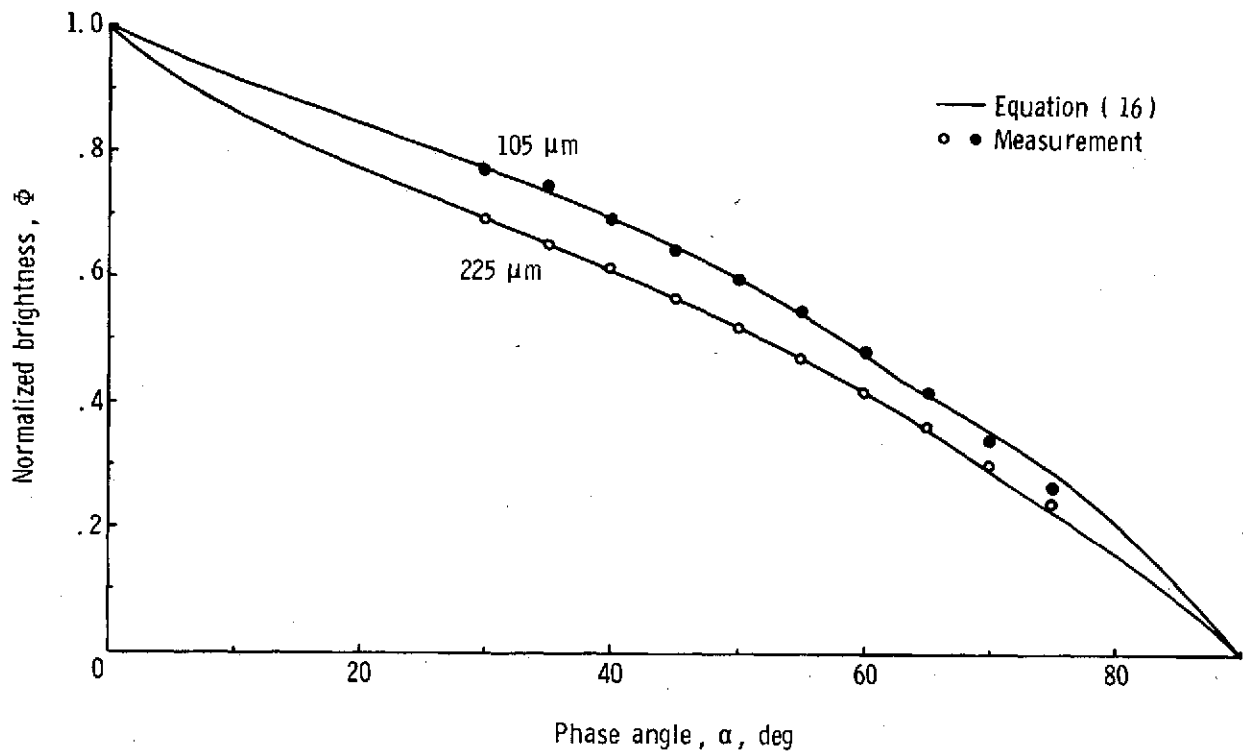
(a) Colorado basalt with mean particle diameters of $105 \mu\text{m}$ and $225 \mu\text{m}$.

Figure 3.- Comparisons between theory and experiment of Minnaert exponent as function of phase angle.



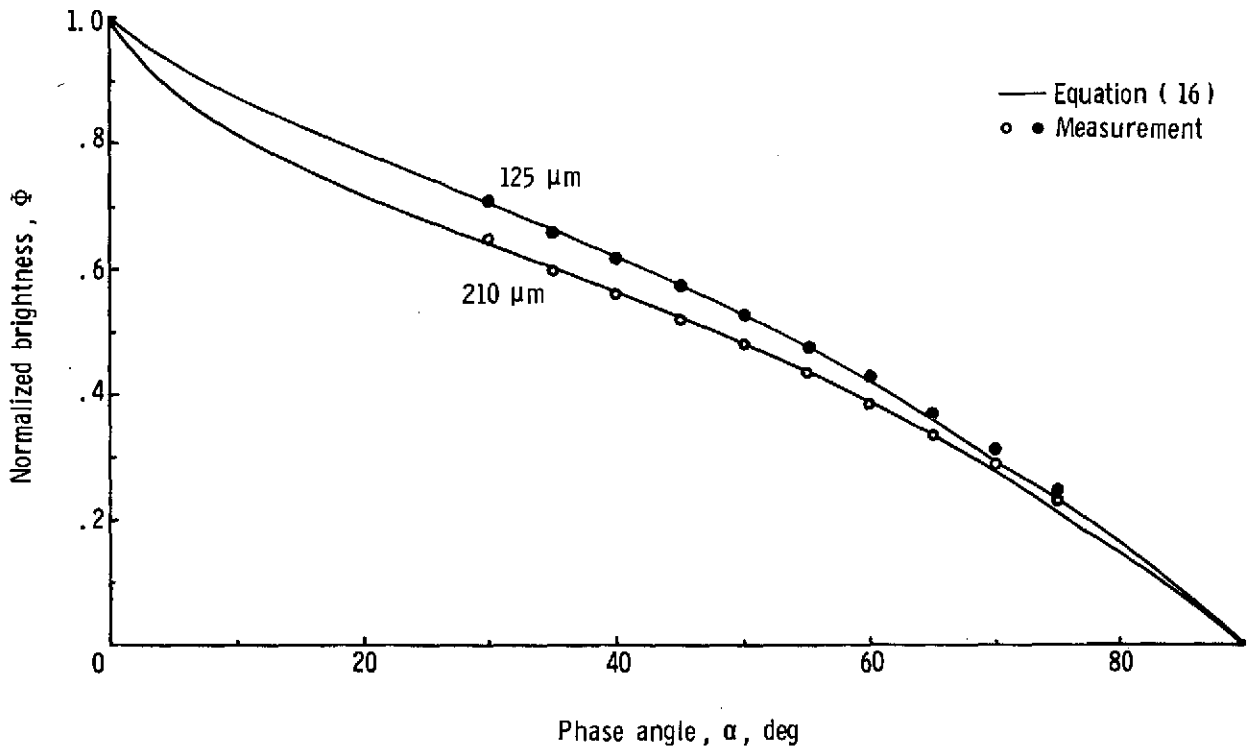
(b) Basalt dune sand with mean particle diameters of 125 μm and 210 μm .

Figure 3.- Concluded.



(a) Colorado basalt with mean particle diameters of 105 μm and 225 μm .

Figure 4.- Experimental and theoretical normalized brightnesses as functions of phase angle for emission angle fixed at 0° .



(b) Basalt dune sand with mean particle diameters of 125 μm and 210 μm .

Figure 4.- Concluded.

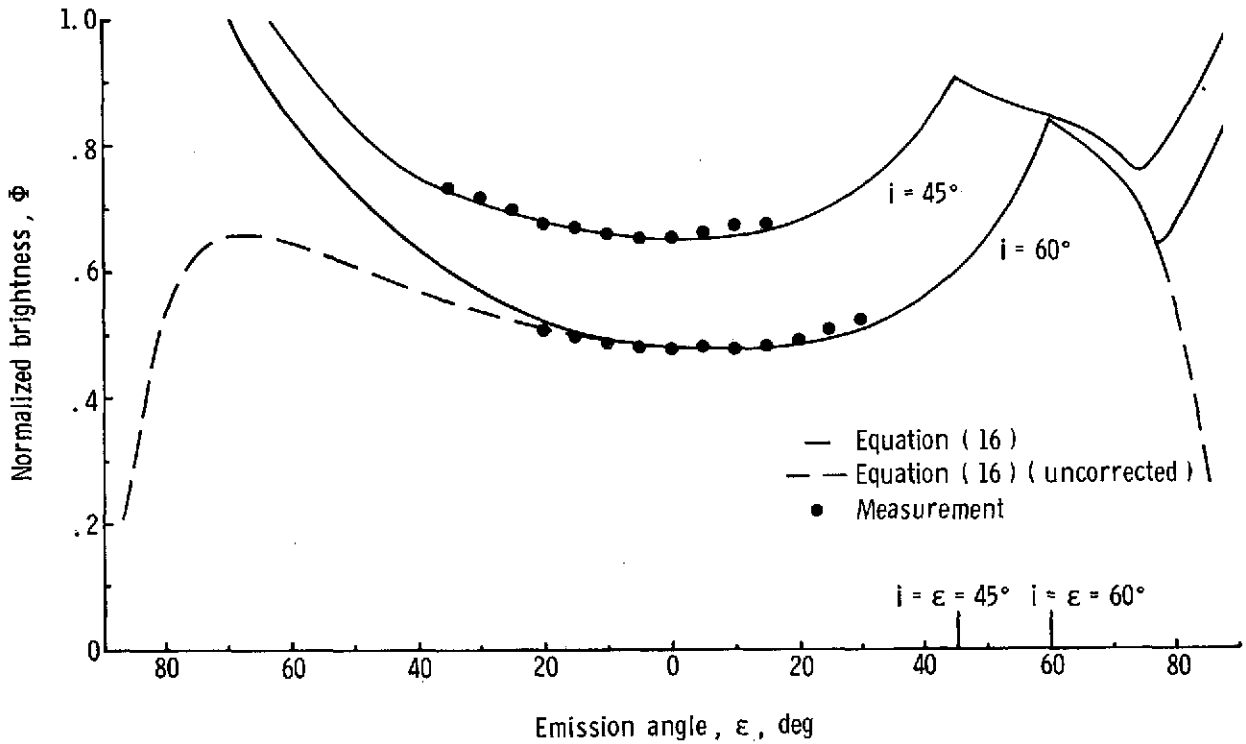


Figure 5.- Experimental and theoretical normalized brightnesses as functions of emission angle for incidence angle fixed at 45° and 60° . Colorado basalt (mean particle size, $105 \mu\text{m}$). The dashed line is the incorrect behavior of the normalized brightness that results from the use of equation (5) without correction for the nonphysical behavior of that expression at large i or ϵ .

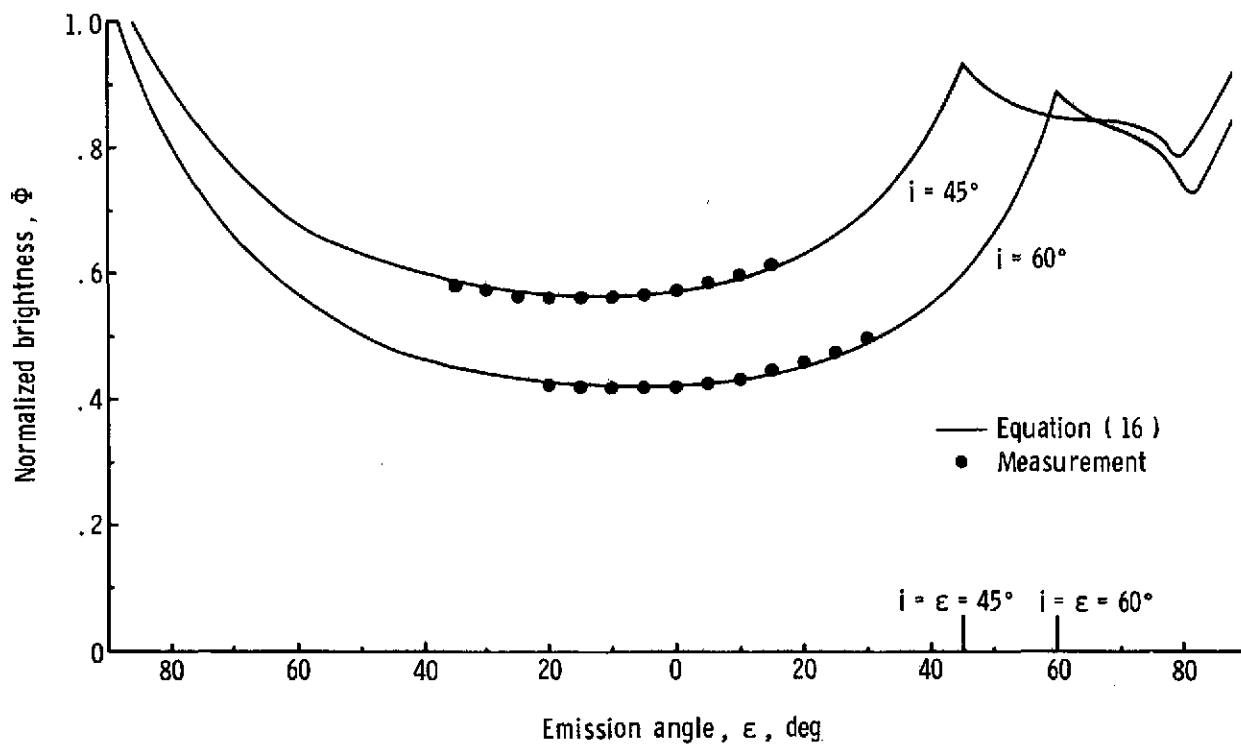
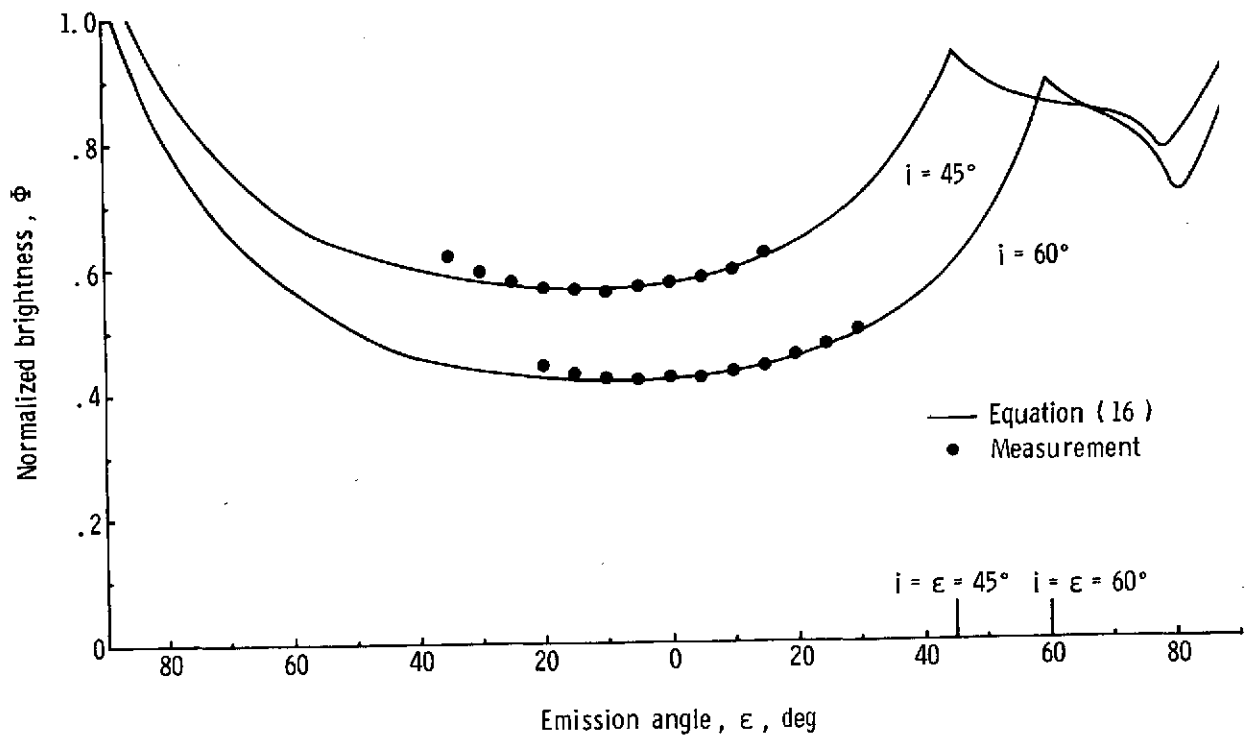
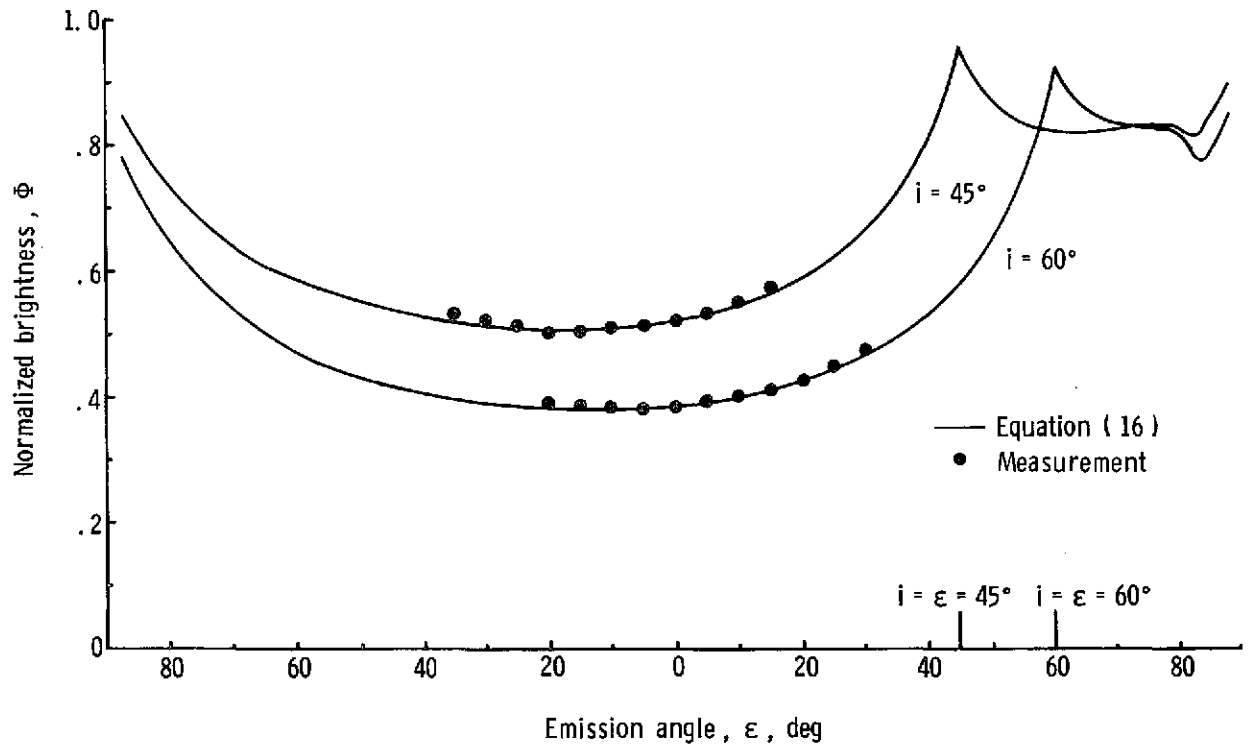


Figure 6.- Experimental and theoretical normalized brightnesses as functions of emission angle for incidence angle fixed at 45° and 60° . Colorado basalt (mean particle size, $225 \mu\text{m}$).



(a) Basalt dune sand (mean particle size, 125 μm).

Figure 7.- Experimental and theoretical normalized brightnesses as functions of emission angle for incidence angle fixed at 45° and 60° .



(b) Basalt dune sand (mean particle size, $210 \mu\text{m}$).

Figure 7.- Concluded.

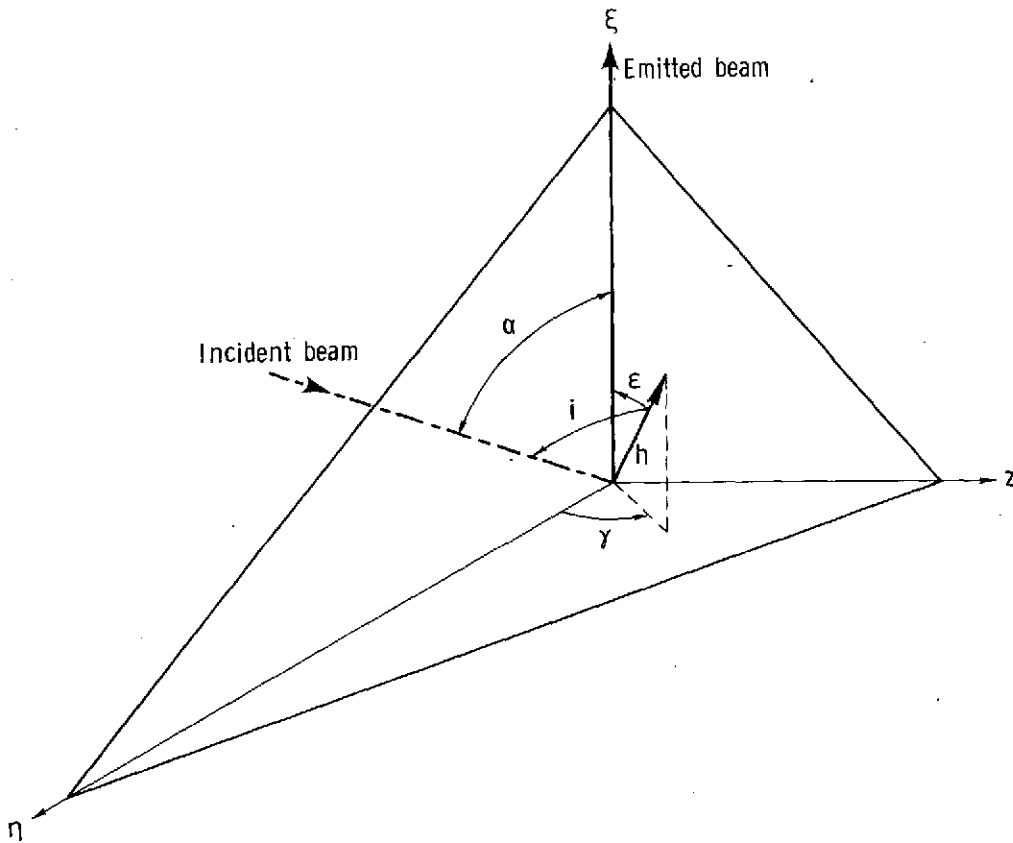


Figure 8.- Scattering geometry for a beam of radiation incident on a particle located at the origin of the ξ, η, z coordinate system.

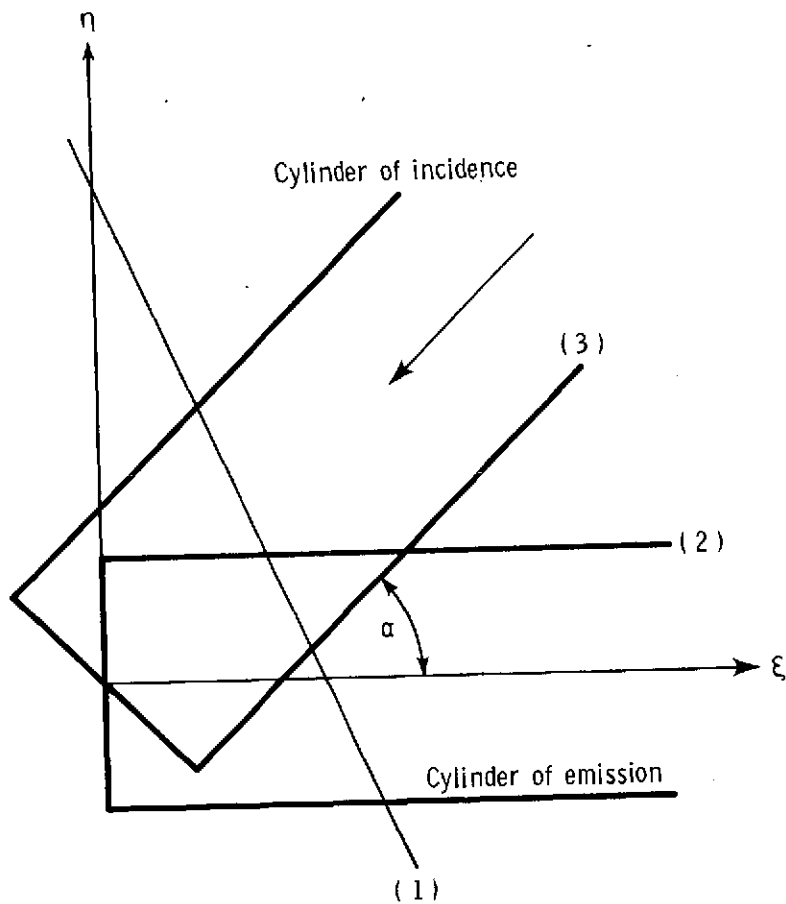


Figure 9.- Intersection with the plane $z = z$ in figure 8 of the material surface (line (1)), the cylinder of incidence, and the cylinder of emission.

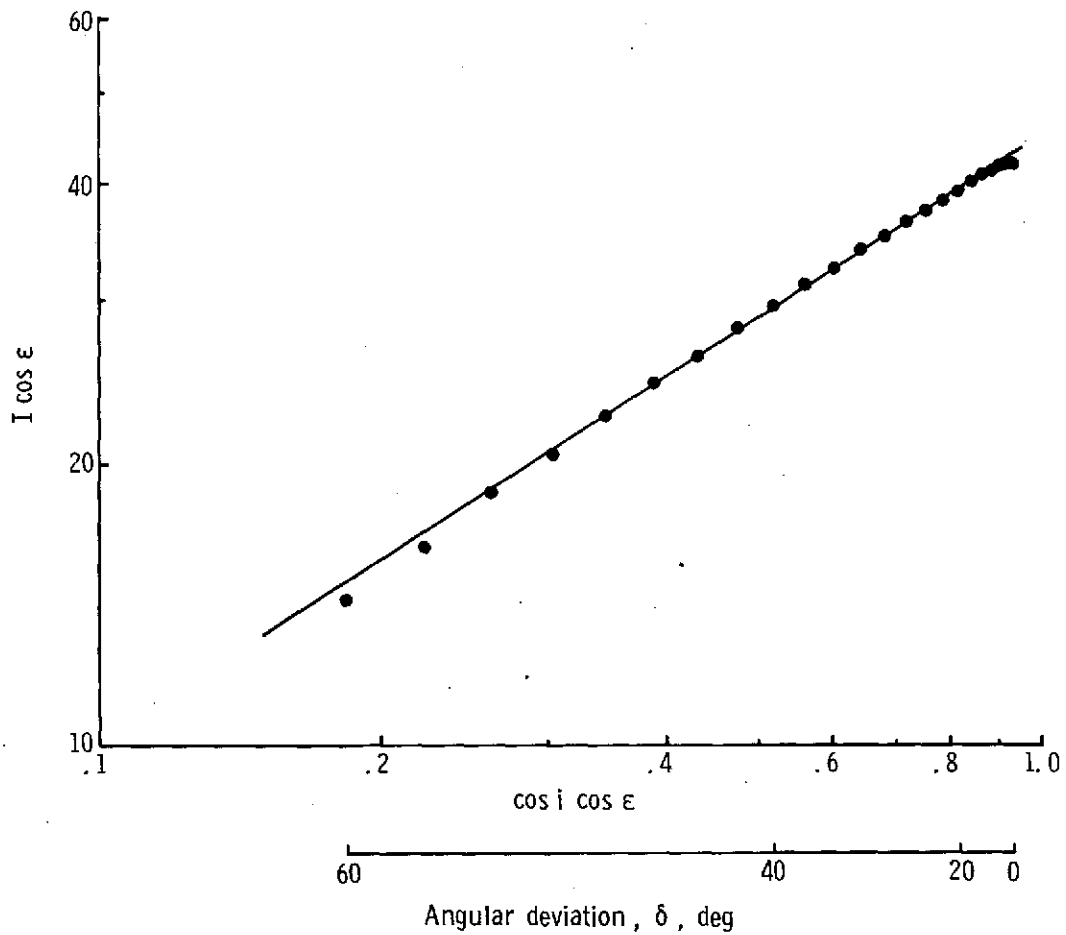


Figure 10.- Minnaert plot of laboratory brightness measurements on basalt dune sand (mean particle size, 210 μm). Phase angle fixed at 30° .